Astron. Astrophys. 358, 242–256 (2000)

ASTRONOMY AND ASTROPHYSICS

(Sub)mm continuum mapping of NGC 6334 I & I(N)

A cobweb of filaments and protostars

G. Sandell

National Radio Astronomy Observatory*, P.O. Box 2, Green Bank, WV 24944, USA (gsandell@nrao.edu)

Received 7 June 1999 / Accepted 16 March 2000

Abstract. We present high resolution (sub)mm continuum maps obtained with the bolometer UKT14 on the JCMT of the high mass star formation complex NGC 6334 I and I(N), the latter also known as Gezari's cold source (Gezari 1982). The maps at 1.1 mm and 800 μm cover the whole northern part of the NGC 6334 complex ($\sim 5' \times 8'$), while the coverage is more limited at 450 μm and 350 μm and centered on NGC 6334 I(N).

The strongest dust emission at all wavelengths originates from a compact source near or coincident with the Ultracompact HII - region NGC 6334 F and the FIR–source and hot core region NGC 6334 I. The dust in NGC 6334 I is hot, $T_d \geq 100$ K, and we derive a total mass (gas + dust) of $\sim 200\,M_\odot$. We resolve Gezari's cold source into a compact (deconvolved FWHM $\sim 10''$) dust source, which appears optically thick even at 1.1 mm. I(N) is embedded in a dense cloud core, $\sim 2.5' \times 1.5'$, with a mass of $\sim 2200\,M_\odot$. *I(N) is clearly a high–mass Class 0 object*. It emits a large fraction of its luminosity in the sub–mm ($L_{bol} \sim 1.7\,10^4\,L_\odot$), it drives a molecular outflow and coincides with a CH_3OH maser, suggesting that I(N) has already formed a hot accretion disk. We derive a total mass of 250–400 $M_\odot$, corresponding to an average gas density 1.6–2.6 10^7 cm^{-3} and a line of sight visual extinction of $\geq 2000^m$, rendering it impossible to detect I(N) even in the thermal or mid–IR.

We also find eight additional compact sub–mm sources. Some of these are probable high–to–intermediate mass protostars, some may be massive cold starless cloud cores that eventually will collapse to form stars. Our sub–mm maps also show a remarkable narrow, lumpy, linear filament, which has no optical or near–IR counterpart. This filament bounds the dust emission to the west and is at least $7'$ (3.5 pc) in length with a width of $\sim 15''$–$20''$. It breaks up into dense condensations with a separation of 3–4 times the width of the filament.

Key words: ISM: dust, extinction – ISM: H II regions – ISM: jets and outflows – ISM: individual objects: NGC 6334 I

1. Introduction

The giant HII region NGC 6334 is associated with a large elongated molecular cloud parallel to the galactic plane (Dickel et al. 1977) at a distance of 1.7 kpc (Neckel 1978). Numerous studies in the radio, near– and far–infrared identify this molecular cloud ridge as a site of active star–formation. McBreen et al. (1979) mapped the region in the far–infrared at 69 μm and identified five centers of star formation within the molecular ridge, and labelled them with roman numerals from I – V. An additional FIR emission region (VI) is much fainter and separated from the main molecular ridge. In their notation, I is the northern–most and densest part of the molecular ridge.

Cheung et al. (1978) mapped most of the molecular/FIR ridge at 1 mm and found mm–counterparts to all the FIR peaks covered by McBreen et al. (1979). The 1 mm map by Cheung et al. (1978) showed an additional peak north of NGC 6334 I that had no radio or FIR counterpart. Gezari (1982) mapped the northern part of NGC 6334 at 400 μm and found that the 1 mm emission region north of I, which he labelled I(N), was brighter than I at 1 mm[1], while both regions had comparable flux density at 400 μm. He concluded that I(N) is a cold, dense protostellar core or a cluster with one or more embedded B stars. I(N) is an intense source of NH_3 emission (Kuiper et al. 1995). From an analysis of the NH_3(3,3) transition Kuiper et al. (1995) derive a gas temperature of ~ 30 K, a density of $\sim 10^6$ cm^{-3} and a total cloud mass of 3,000 $M_\odot$. Although no free–free emission has been found towards I(N) (Rodríguez et al. 1982), it is a site of H_2O and CH_3OH maser emission (Moran & Rodríguez 1980, Menten & Batrla 1989, Norris et al. 1993, Kogan & Slysh 1998) and drives a molecular outflow (McCutcheon et al. 2000), confirming that star formation is already in progress.

NGC 6334 I is the brightest FIR source in the northern part of NGC 6334 and coincides with an Ultra–Compact HII–region (UC HII), NGC 6334 F (Rodríguez et al. 1982, Gaume & Mutel 1987; Jackson et al. 1988) and a hot core, which is an extremely rich molecular line source (Bachiller & Cernicharo 1990, Nummelin et al. 1998, McCutcheon et al. 2000). NGC 6334 I is very

* The National Radio Astronomy Observatory is a facility of the National Science Foundation operated under cooperative agreement by Associated Universities, Inc.

[1] We find that NGC 6334 I is stronger than I(N) at all wavelengths, when the sources are observed with high spatial resolution. Gezari's claim that I(N) is stronger than I at 1 mm was due to beam dilution, but nevertheless his conclusions were basically sound.

bright and compact in the mm and sub–mm regime, and has been used as a secondary calibrator for sub–mm photometry at JCMT (Sandell 1994). It drives two molecular outflows (Bachiller & Cernicharo 1990, McCutcheon et al. 2000). The outflows are also seen in vibrationally excited H_2 (Davis & Eislöffel 1995, Persi et al. 1996) and as NH_3 maser spots (Kraemer & Jackson 1995) coinciding with the shocked H_2 emission. High resolution FIR studies by Harvey & Gatley (1983) revealed two very luminous red sources: IRS−1, which is the exciting source for the UC HII region, and IRS−2, which they suggested might be a protostar. Studies of molecular masers confirm the presence of two activity centers. The OH, CH_3OH and H_2O maser emission is centered on F, the UC HII region (Gaume & Mutel 1987, Norris et al. 1993, Ellingsen et al. 1996, Norris et al. 1998, Forster & Caswell 1989). In addition CH_3OH also shows a second activity center, possibly associated with IRS−2 (Ellingsen et al. 1996, Norris et al. 1998).

In this paper we concentrate on the sub–mm dust continuum emission from the region around NGC 6334 I & I(N). The dust emission is a good tracer of high density gas, because the emission is generally optically thin in the mm and sub–mm regime. The dust emission therefore provides better contrast between high and low density gas than most molecular lines. Furthermore, mapping the dust emission can be done much faster than mapping the cloud in an optically thin molecular line. However, the main drawback with continuum observations is that they do not provide kinematic information, and in order to understand the nature of the cloud condensations that we see in continuum we also need molecular line observations. A parallel paper by McCutcheon et al. (2000) therefore discusses molecular line observations of the same field and some data are shared between the two projects.

2. Observations and data reduction

2.1. Observations

Most of the observational data were obtained with the common user bolometer UKT14 on the 15m James Clerk Maxwell Telescope[2], on Mauna Kea, Hawaii, during two observing runs: 1990 March 13–15, and 1991 March 25–27. Some additional maps were acquired in 1993, May 26–28. All photometry and mapping was carried out with the common user bolometer, UKT14. UKT14 is a sensitive, ^{3}He–cooled, one channel bolometer with a filter wheel and a variable iris that permits diffraction limited observations at wavelengths from 1.1 mm - 350 μm. The measured diffraction limited HPBWs were $18\farcs5$ at 1.1 mm, $13\farcs5$ at 800 μm, $8\farcs5$ at 450 μm, and $7\farcs8$ at 350 μm. For longer wavelengths the optics over–illuminate the primary. The instrument is described in more detail by Duncan et al. (1990). Details of photometry observing techniques and reduction are also presented by Sandell (1994). Calibration was derived from observations of Uranus, Mars, and the secondary calibrators IRAS16293−2422, G5.89−0.39, and NGC 6334 I (Sandell 1994). NGC 6334 I is within the field that has been mapped, and therefore provides an additional check on the calibration accuracy of the (sub)mm maps. At 1.1 mm and 800 μm it has well determined flux densities, which are accurate $\leq$ 10%. At 450 μm and 350 μm the uncertainties are much larger, probably of the order of 20% (Sandell 1994). During the mapping in 1993, all the calibration was based on NGC 6334 I alone. Continuum maps in on–the–fly mode, i.e. continuously scanning in azimuth while chopping in the scan direction, have been obtained at 1.1 mm, 800 μm, 450 μm, 350 μm, as well as at 1.3 mm with the map from McCutcheon et al. (2000).

The weather conditions were excellent during the first two nights in 1990. The precipitable water vapor was 0.5–1 mm with photometric and stable sky conditions were surprisingly stable. We therefore started mapping the I(N) region at 450 μm based on the low spatial resolution maps published by Gezari (1982). Some of the maps were too small, which made the data reduction rather complicated. The reduction of the maps will be described in more details below.

In 1991, the sky conditions were rather marginal with 2–5 mm of precipitable water vapor, which is hardly sub–mm observing weather. Most of the observations were therefore done at 1.3 mm and 1.1 mm, but we did acquire a few maps of NGC 6334 I at 450 and 350 μm, when the precipitable water vapor was $\sim$ 2 mm. These maps have noise levels about 5 times larger than the much deeper maps centered on I(N), which had noise levels of 3–6 Jy/beam for integration times of 1 sec/map point. Because NGC 6334 I is very bright in the sub–mm, the 450 μm–map is still useable, but the 350 μm–map is very marginal and has been added in mostly for cosmetic reasons.

The dust emission is spatially quite extended in the northern part of NGC 6334. One therefore needs to map rather large areas. In order to keep the mapping time down to reasonable limits, i.e. less than two hours, we have mapped the region with overlapping sub-fields using short integration times. In most cases we compromised on the amount of oversampling. At 1.3 mm the sample spacing was $6''$ and the chop throws used were $60''$ and $48''$. At 1.1mm two of the maps were sampled with a $7''$ spacing (both covering I & I(N)) and a $56''$ chop throw, while one map of the northernmost part of the cloud was obtained with a sampling of $6''$ and a chop throw of $48''$. All maps obtained in 1993 at 800 μm were taken with $4''$ spacing and a $40''$ chop. One 800 μm-map was retained from the 1990 observing run. This map was done with a $50''$ chop and a $5''$ sampling. At 450 and 350 μm all maps were obtained with $3''$ spacing and a $30''$ chop throw. The generally rather short chop throws ($30''$–$60''$) are really good in cancelling the sky noise and remove variations in sky background. However, the downside is that we are not sensitive to extended emission of spatial scales larger than a few times the chop throw (see e.g. Emerson et al. 1979). This is unimportant as long as we study compact structures, but is more than likely to affect the total integrated intensities of

[2] The James Clerk Maxwell Telescope is operated on a joint basis between the United Kingdom Particle Physics and Astronomy Research Council (PPARC), the Netherlands Organisation for the Advancement of Pure Research (ZWO), the Canadian National Research Council (NRC), and the University of Hawaii (UH).

the surrounding extended molecular cloud. Furthermore, it will underestimate the short wavelength observations more than the ones at long wavelengths. At short wavelengths the HPBW is small, and it takes longer to map the same area, and the sky opacity is always much higher, which make the maps more noisy. We use short chop throws to cut down the area we need to map and also because large chop throws cause beam degradation due to coma.

In a different experiment, we used the double sideband heterodyne receiver, RxB2, tuned to relatively line free region with the two sidebands centered on 348 GHz and 356 GHz. These observations were done on March 30, 1991 in good, stable weather conditions. The receiver had an IF frequency of 3.94 GHz, and the local oscillator was centered at 351.99 GHz. We added a 520 MHz bandpass filter to restrict the continuum bandpass to approximately the bandwith as used by our spectral line backend, DAS, which was 500 MHz. We observed with RxB2 exactly the same way as we do photometry with UKT14, i.e. we used chop throws of 60″ and 120″ with a 4 Hz chop frequency. The output of the receiver was fed through the UKT14 backend. Beam maps and photometry of Uranus were used for calibration. Since RxB2 has a three position calibration unit (hot, cold, and sky), we used the internal receiver calibration to directly measure the sky opacity in the direction of the objects that were observed. We did three sets of photometry on NGC 6334 I and one on NGC 6334 I(N). These were interleaved with position switched spectra of both I and I(N). The latter were taken to estimate the contribution from line emission in the observed band. NGC 6334 I has such a rich molecular line spectrum, see e.g. McCutcheon et al. (2000), that it is impossible to find a 500 MHz band completely free of lines. By integrating over the observed spectra we find that the molecular lines contribute with $\sim$ 2 Jy to the continuum flux density. Since the observed flux density was 53.0 $\pm$ 1.6 Jy/beam, the true continuum flux density is 51.0 $\pm$ 2 Jy/beam (HPBW = 13.″3), i.e. even in our "line free" narrow band continuum observations we therefore measure a 4% continuum excess due to the contribution from spectral line emission in our passband. When we compare these observations to the 850 μm broadband UKT14 photometry (Sandell 1994), we derive a line contamination of 8 $\pm$ 4% at 850 μm. Since we have no observations for any other filter, we assume that the spectral line contamination is similar at all wavelengths. No line emission was observed towards NGC 6334 I(N) ($S_{352\mathrm{GHz}}$ = 28.3 $\pm$ 1.0 Jy/beam), and therefore broad band bolometer observations here measure the true continuum, uncontaminated by spectral line emission.

2.2. Data reduction

The initial reduction of all maps has been done using the the NOD2 software package (Haslam 1974) adapted for JCMT. The maps have been calibrated in a standard fashion. The extinction is derived from photometry of primary and secondary calibrators and by crosschecking the results with the 1.3mm tau meter at CSO (see e.g. Sandell 1994). At long wavelengths, the conversion factors to Jy/beam have been derived from photometry alone, while the maps at 450 and 350 μm have been calibrated with conversion factors derived from maps of planets obtained with the same chop throw and sampling interval. All maps are calibrated in Jy/beam.

The pointing was always checked on a standard pointing and calibration source before and after each map. Any pointing drifts in the maps have been removed to first order by assuming a linear drift of the pointing errors throughout the map. Unfortunately G5.89−0.34, which was extensively used as a pointing source during the first observing run, had at the time an incorrect position of several arcseconds, affecting the deduced absolute positions of the sources as well as the magnitude of drift throughout the maps. We therefore first analyzed all maps, which simultaneously cover both I & I(N), so that we cloud derive a more accurate position for I(N), by measuring its coordinates relative to I. It should be noted, however, that the position of NGC 6334 I, which serves as the primary astrometry standard for our maps, is in itself uncertain by a few arcseconds. The UC HII region is extended by several arcseconds and the positions quoted from VLA observations vary depending on frequency or whether the observers quote the peak or centroid position. The sub–mm position adopted by us (see Table 1) is a compromise between the position of the UC HII region F and the 7 mm dust emission mapped by Carral et al. (1997).

The dust emission from NGC 6334 is very extended. Therefore, if our maps do not fully cover all the emission along the scan direction, the standard NOD2 reduction will cause negative features in the map, which repeat every chop throw. In several cases this cloud not be avoided, and we therefore carefully inspected the dual beam map and blanked out all emission that was not covered by both beams in order not to contaminate the emission in the central regions of the restored map. However, for some maps this cloud not be done, because they were centered on regions with extended emission and not big enough to go off source. These maps would therefore have to be disregarded, if we would rely solely on NOD2 reduction. We have therefore based most of our analysis on DBMEM, the dual beam maximum entropy reduction package written for JCMT by John Richer (Richer 1992). NOD2 is only used for initial map preparation and to provide calibration for the DBMEM–maps.

The DBMEM reduction starts from calibrated, baseline subtracted, and unrestored dual beam maps in Az/El, i.e. horizontal coordinates. The maps are reconstructed and coadded with DBMEM in the equatorial coordinate plane. The advantage of DBMEM is that it can cope with maps that do not cover a source in both beams. The other advantage of DBMEM is that it deconvolves the data, i.e. removes the dirty beam, and hence we can significantly improve the resolution, especially for heavily oversampled maps with good signal–to–noise (S/N). DBMEM is very memory and CPU intensive, and we therefore had to use synthetic beams rather than high dynamic beam maps. The DBMEM input beams were created from measured beam maps by fitting them with two component circular Gaussians. After deconvolving the maps, we created model beams, where the the first component is a narrow Gaussian representing the main beam, while the error beam is modelled by a low amplitude

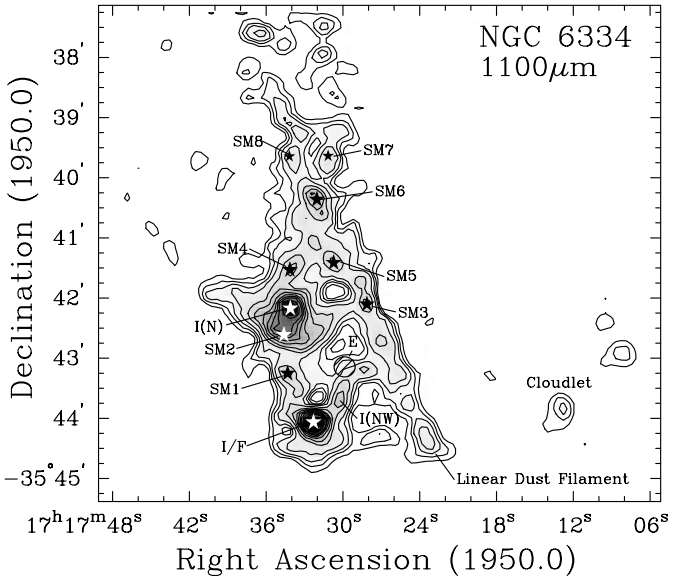

Fig. 1. Overview of the dust emission at 1100 μm from the NGC 6334 I & I(N) area. The 1100 μm has been reduced with DBMEM and cosmetically smoothed with a 6″ Gaussian. The peak flux in the map is 4.95 Jy/beam. The continuum emission is plotted in greyscale and overlayed with contours. The contour levels are 0.04, 0.08, 0.125, 0.2, 0.35, 0.5, 0.75, 1.0, 1.25, 1.5, 2.0, and 2.5 Jy/beam. The FIR source NGC 6334 I and the UC HII region F both coincide with the strong continuum source in the southern part of the map. The cold source I(N) discovered by Gezari (1982) is $\sim 114''$ north of I. The HII region E is plotted with a hatched circle that show the approximate size of the H II region. The positions of all other continuum sources are marked with a black or white star symbols and are labelled with the prefix SM.

extended Gaussian. This ignores any additional structure in the error beam. For most of our maps this beam approximation is more than sufficient, but it does not appear to work very well close to NGC 6334 I, which is exceedingly bright. Here the DBMEM reduction appears to suppress emission very close to the source, and some of the structure, maybe up to a radius of 30″–40″ from NGC 6334 I is not very reliable.

DBMEM is sensitive to calibration and pointing errors and may not produce reliable results if the errors are too large. It also requires that the baseline level in the dual beam map is accurate. This is no problem if the emission is covered by both beams, since then the mean level in the map is zero. If neither beam is completely off source it can be very difficult to determine the baseline level and any errors in the baseline level may cause DBMEM to produce spurious sources. Most fields were therefore analyzed a number of times by trying different noise levels and map combinations. In this process we also adjusted the baseline levels and corrected for small pointing shifts between maps. At some frequencies we cloud not simply reduce all the maps in one go, but had to reduce them as separate subfields, either because maps were not overlapping or because the amount of data were so large that we ran out of memory on our workstation. In these cases the maps were mosaiced together using the MIRIAD task LINMOS (Sault et al. 1995). The final acceptance of a map was made by judging how reliable it looked relative to the NOD2 map and by making sure that maps of the same regions at different wavelengths showed the same features. The only region where we have differencies in morphology between maps is in the immediate vicinity of NGC 6334 I, and as mentioned above, this is most likely due to incomplete removal of residual error lobe pattern.

These "raw" DBMEM images have been baseline subtracted and recalibrated using integrated fluxes deduced from calibrated NOD2 maps. Whenever possible several reference regions were used for each map. We have also smoothed the maps with a Gaussian beam to enable us to go back to a Jy/beam intensity scale or in some cases applied a marginal "cosmetic" smoothing. Since JCMT is by no means a perfect telescope at short wavelengths, we subtracted out the error lobe contribution from the NOD2 maps by assuming that the error lobe contributes to 6% of the power at 1.3 mm, 10% at 1.1 mm, 20% at 800 μm, 50% at 450 μm, and 65% at 350 μm[3] over a square $60'' \times 60''$ area, as measured from beam maps of planets and consistent with our model beams. The DBMEM reduced and mosaiced maps are shown in Figs. 1 and 2.

3. Results

3.1. Large scale morphology

The 1.1 mm map, presented in Fig. 1, gives a good overview of the region. The northern–most part of the map has a much higher noise level, but we can see that the emission still continues to the north outside the area mapped by us. There is no dust emission in the western part of the map, except for a faint "dust–cloudlet" $\sim 240''$ west of NGC 6334 I, seen in both the 1.3 mm and the 1.1 mm maps. Some additional faint emission blobs in the same area are likely to be spurious, i.e. artifacts from the DBMEM reduction. The map shows that the dust emission is concentrated to two main emission centers, I and I(N), and that the dust emission is sharply bounded to the west by a long narrow linear filament. Additional ridges connect this filament to I and I(N). These ridges and lumps give the sub–mm images the appearance of a cob web. The crossing points are regions of intense sub–mm emission, which appear to contain embedded high to intermediate mass proto–stars or clusters of protostars. These regions, especially in the south, are connected by lumpy ridges of dust emission. In addition to the two strong sub–mm sources NGC 6334 I and I(N), we identify eight additional sources. These are labelled with the prefix SM in Fig. 1.

3.2. The linear filament

The narrow straight filament (width $\sim 15''$–$20''$) that bounds the dust emission to the west is especially striking. This fila-

[3] We would expect the error lobe contribution to be substantially higher at 350 μm, but this is the value we derived from a map of Uranus. The most likely explanation for the low error lobe contribution is that a relatively large fraction of the error lobe is subtracted out by the short 30″ chop throw used for all 350 μm–maps.

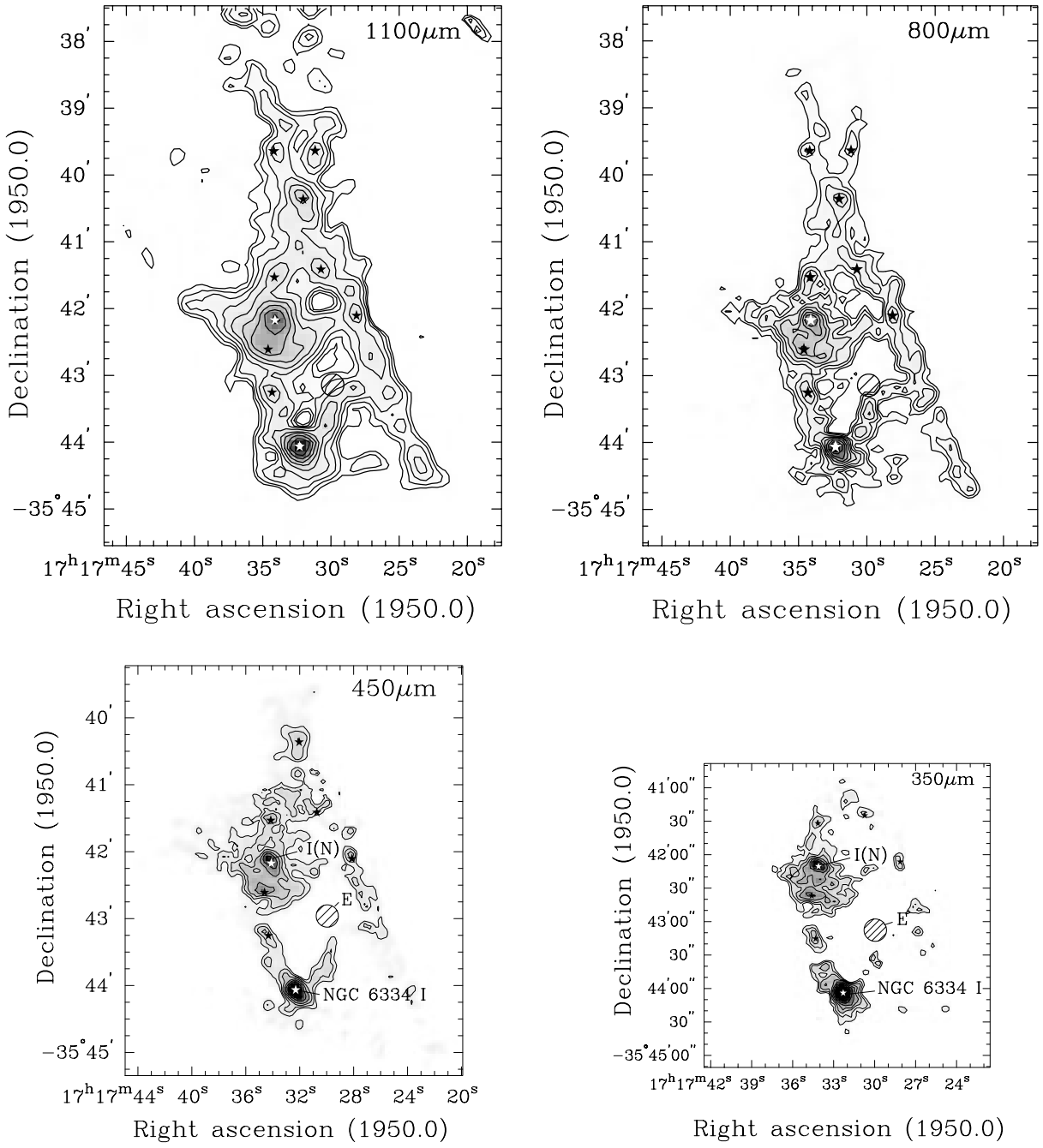

Fig. 2. Continuum maps at 1100 μm, 800 μm, 450 μm, and 350 μm plotted to the same angular scale in grey scale overlayed with contours. The 1100 μm and 800 μm–maps are restored with a 6″ Gaussian beam and have peak flux densities of 4.95 Jy/beam and 25.2 Jy/beam, respectively. The 450 μm and 350 μm–maps are restored with a 3″.5 Gaussian beam and have peak flux densities of 73.1 Jy/beam and 169.7 Jy/beam, respectively. The contours levels are plotted with ten logarithmic contours with the lowest contour at 5% of the peak flux density and the highest at the peak flux density. The sub–mm sources from Fig. 1 are marked with star symbols and the hatched circle marks the position and size of the HII region E. Note that the 450 and 350 μm–maps have good S/N only around I(N). The 450 μm mosaic appears to have some position errors due to the mosaicing. SM 1, SM 5, and SM 6 (see Fig. 1) are somewhat unreliable in the 450 μm–map, because they all fall in overlap areas between sub–maps.

ment has the appearance of an ionization front, e.g. similar to the Orion bright bar, yet there is nothing visible in optical plates of the region, nor in the near–IR surveys. The high resolution "True colour" JHK image by Tapia et al. (1996) shows that the extinction falls off rapidly to the west, approximately where we see the filament, but the near–IR images do not show a sharp boundary between the low and high opacity region. The filament is narrow and lumpy, and appears to continue to the south, outside the area covered by our maps. The 800 μm-map (Fig. 2), which has higher dynamic range in the north, shows that it still

Table 1. Coordinates and deconvolved sizes (FWHM) of "compact" sources in the NGC 6334 I and I(N) region, derived from Gaussian fits to the DBMEM reduced images.

SOURCE	$\theta_{s1} \times \theta_{s2}$ ($''$)	PA ($^\circ$)	α(1950.0) h m s	δ(1950.0) $^\circ$ $'$ $''$	α(2000.0) h m s	δ(2000.0) $^\circ$ $'$ $''$
I	10×8	$+35$	17 17 32.2	$-$ 35 44 04.0	17 20 53.35	$-$ 35 47 01.5
SM1	20×9	$+25$	17 17 34.32	$-$ 35 43 15.4	17 20 55.44	$-$ 35 46 12.7
SM2	13×8	$+80$	17 17 34.61	$-$ 35 42 36.8	17 20 55.71	$-$ 35 45 34.1
SM3	15×8	$+0$	17 17 28.13	$-$ 35 42 06.4	17 20 49.22	$-$ 35 45 04.2
I(N)	11×8	$+60$	17 17 34.08	$-$ 35 42 10.5	17 20 55.17	$-$ 35 45 07.8
SM4	11×9	-40	17 17 34.15	$-$ 35 41 32.1	17 20 55.22	$-$ 35 44 29.4
SM5[a]	17×10	$+55$	17 17 30.73	$-$ 35 41 24.9	17 20 52.09	$-$ 35 54 22.5
SM6	15×11	$+40$	17 17 32.04	$-$ 35 40 21.8	17 20 53.18	$-$ 35 43 06.4
SM7[b]	27×14	-12	17 17 31.16	$-$ 35 39 38.3	17 20 52.18	$-$ 35 42 35.9
SM8[b]	16×11	-40	17 17 34.19	$-$ 35 39 38.7	17 20 55.21	$-$ 35 42 36.0

[a] SM 5 is not seen at 800 μm, and not confirmed at 450 μm because it falls into an overlap area between two sub–maps.
[b] Poor positional accuracy and some inconsistency between the 1.3 mm, 1.1 mm and 800 μm–maps.

continues straight into the dust cloud even though here the dust emission also curves to the north. The filament bends off to the east, and then makes a sharp turn back approximately at the position of SM 8 (see Fig. 1 and Table 1). The northermost part of the filament is again perfectly aligned. This filament appears to coincide with the boundary of high visual extinction, as mapped by Straw & Hyland (1989) from their near–IR survey of the NGC 6334 complex. Their high extinction region also turns towards north east as well as westward at a declination of $\sim -35^\circ$ $40'$, and continues to the south–west as far as NGC 6334 V. The total length of the filament, as seen in our 800 μm–map is $\sim 7'$ (3.5 pc), but it is possible that it may follow the high extinction boundary all the way to NGC 6334 V. Nevertheless, it covers a large distance on the sky and is remarkably straight. There is no sign of bending, or curvature, apart from the apparent lumpy structure of the filament.

3.3. Cores, ridges and holes

NGC 6334 I is by far the strongest source at all wavelengths, and barely resolved in our maps. It is surrounded by relatively little extended emission, although there is a ridge of emission extending towards the more evolved UC HII region E, and continuing past it to connect with the linear filament. There is also another dust bridge that connects I to the extended cloud core surrounding I(N). In the sub–mm I appears as a single source, but high resolution molecular line and maser observations shows that it harbours at least two young stars. Our maps of the I(N) region resolve at least two different sites of star formation, both of which may harbour multiple sources.

The I(N) region continues to the north through another bridge of emission, which is fainter than the one to the south. This bridge merges in the north into a more extended region bounded to the west by the linear ridge. The I(N) region connects through another dust bridge to the west, which terminates more directly on the linear filament. Further north the emission gets fainter, and the dust peaks appear less point–like and fainter. These may be regions, which are both colder and less massive, and which have not yet formed any stars.

There seems to be several empty regions void of gas and dust, bounded by I, I(N) and the linear filament. These regions void of dust stand out even clearer on the 450 and 350 μm–maps. Overall, there is very little dust emission east and northeast of NGC 6334 I, until we get up to I(N) which shows a spur of emission extending almost straight east. The region south of I is also devoid of emission. The location of the more evolved HII region E, powered by a cluster of B–type stars (Tapia et al. 1996), on a ridge of emission with areas void of gas both to the north–east and the south–west would suggest that the area cloud have been cleared by an energetic wind from E, which now is almost void of dust. However, the morphology of the voids do not lend much support to such an idea. This looks more like a pre–existing structure, which was present even before E was formed.

3.4. Compact sources

We can identify more than 10 cores in the 1.3 mm – 800 μm maps, which appear to be massive compact cloud cores. Table 1 lists average source sizes and positions for 10 of these cores ordered from south to north, which have been identified on at least two different maps. The positions are all relative to our adopted position of NGC 6334 I (see Sect. 2.2). The relative positions should be accurate to $\sim 2''$ except for the northern part of the cloud, which was not covered by our 450 and 350 μm–maps. The S/N and positional accuracy of these sources are much poorer than for the rest of the cloud. Table 2 gives flux densities derived from Gaussian fits for the sources that we could fit with a Gaussian. For the fainter sources the flux estimates are rather uncertain, because the fits at long wavelengths tend to give rather large source sizes. In order to ensure that we sample the same region, we have crudely corrected these fluxes so that they refer to the same source size.

Table 2. Integrated fluxes of compact sources and the I(N) cloud core.

SOURCE	S(1.3mm) [Jy]	S(1.1mm) [Jy]	S(800 μm) [Jy]	S(450 μm) [Jy]	S(350 μm) [Jy]
I	24.1 ±2.4	22.8 ±4	90 ±20	700 ±70	1130 ±200
SM1	1.8 ±0.8	2.7 ±0.5	10.9 ±1.1	56.8 ±12	150 ±30
SM2	–	–	21.0 ±4.0	52 ±10	95 ±20
SM3	4.6 ±.5	2.7 ±0.3	11.4 ±1.1	37 ±3.7	90 ±18
I(N)	14.2 ±2.0	17.1 ±2.0	46.0 ±5.0	230. ±22	330. ±60
SM4	0.6 ±0.4	1.1 ±0.4	7.0 ±0.7	45 ±8	66 ±13
SM5	1.3 ±0.6	1.3 ±0.3	–	–	–
SM6	1.1 ±0.2	3.4 ±0.4	9.4 ±0.9	29 ±6	–
SM7	1.2 ±0.5	2.8 ±0.8	6.8 ±1.0	–	–
SM8	0.7 ±0.3	1.4 ±0.5	5.5 ±1.1	–	–
I(N) Cloud	44.4 ±4.4	74.8 ±7.5	230.5 ±46	1455 ±440	3090 ±930

4. Simple analysis of the dust emission

We will use a simple isothermal model to derive dust masses and densities of the sub–mm sources that we have identified in our maps. We can write the flux density S_ν at at a frequency ν due to thermal emission from dust grains with a temperature, T_d, as

$$S_\nu = \Omega_s B_\nu(T_d)(1 - e^{-\tau_\nu}) \quad (1)$$

Here Ω_s is the source solid angle of the dust emitting region, $B_\nu(T_d)$ is the Planck function, and τ_ν is the optical depth of dust at the frequency ν. Because the dust is largely optically thin in the sub–mm we can assume that Ω_s is constant and independent of frequency. We also make the assumption that the bulk of the dust is at a single temperature T_d. The dust optical depth is proportional to the dust mass opacity κ_ν, which is generally expressed as a power law in the FIR and sub–mm (see e.g. Hildebrand 1983, Emerson 1988). We can therefore write

$$\tau_\nu = \tau_o \left(\frac{\nu}{\nu_o}\right)^\beta \quad (2)$$

where τ_o is the dust optical depth at frequency ν_o and β is the dust emissivity index.

Most of our sub–mm sources have no FIR counterparts. One of the reasons is because NGC 6334 I is so exceedingly bright in the FIR, that it makes it difficult to detect nearby fainter sources. The second reason is that most of the sub–mm sources in NGC 6334 are relatively cold and therefore faint in the FIR, especially when observed with large beams. This means, however, that that we cannot accurately determine the temperature. If we assume that the Rayleigh–Jeans approximation is valid, i.e. $h\nu/kT_d \ll 1$, and that the dust emission is optically thin, we can see that Eq. 1 now predicts

$$S_\nu \propto \Omega_s \tau_\nu \times T_d \quad (3)$$

Even though the Rayleigh-Jeans approximation is not exactly valid in the (sub)mm regime, S_ν is roughly proportional to T_d, Ω_s, and τ_ν, and it is easy to see that sub–mm observations do not enable us to separate the dust optical depth from the temperature; they are strongly coupled as long as the dust emission is optically thin. We can, however, make a guess about the dust temperature, because we know the temperature of the gas from molecular line studies. For the high gas densities that we see in NGC 6334, we expect the gas and the dust to be closely coupled (Goldreich & Kwan 1974). Therefore the dust temperature will be close to that of the molecular gas. Furthermore we can use FIR data to constrain the total luminosity of our sources, in the same way Wright et al. (1992) did in their study of Orion.

We have therefore largely followed the same technique as used by Wright et al. (1992) and done least–squares fits to Eq. 1, constrained to the measured source size and the dust temperature. We give a limit for the source size, with the upper limit being the measured size at 450 or 350 μm, but note that these are upper limits to the true source size, which depend on how well we removed the telescope beam for the data. We also give a range for the dust temperature, which will cause the least squares fit to find a physically plausible solution.

Once we derive a plausible fit which gives us β and T_d, we compute the total dust and gas mass, M_{tot}, from the fit using

$$M_{tot} = 1.88 \times 10^{-2} \left(\frac{1200}{\nu}\right)^{3+\beta} S_\nu (e^{0.048\nu/T_d} - 1) D^2, \quad (4)$$

which is just a simplified version of Eq. 6 of Hildebrand (1983). This assumes a gas–to–dust ratio of 100 and standard Hildebrand opacities (i.e. $\kappa_{1200\mathrm{GHz}}$ = 0.1 cm^2 g^{-1}). In this equation D is the distance in units of [kpc] and $\mathrm{M_{tot}}$ is in [$\mathrm{M_\odot}$]. Once we know the mass and radius of the emitting cloud we can compute the average gas density

$$\langle n \rangle = 2.52 \times 10^8 \frac{M_{tot}}{(\theta D)^3} \ \mathrm{cm}^{-3}, \quad (5)$$

where θ is the diameter of the cloud in arcseconds, and we have taken the gas mass/H_2 molecule to be 4.5×10^{-24} gm.

Hildebrand (1983), recommended a value of β = 2 for wavelengths, $\lambda > 250\,\mu$m (i.e. ν = 1200 GHz) and β = 1 for shorter wavelengths. His recommendation for κ_o, typically defined at 250 μm (1200 GHz), i.e. $\kappa_{1200\mathrm{GHz}}$ = 0.1 cm^{2}g^{-1} is by far the most frequently used dust opacity in sub–mm studies, but subject to large uncertainties. Hildebrand (1983) quotes an uncertainty of a factor of 3–4, while Draine (1990) shows that it is

more like a factor of 10, although some dust models are perhaps not very realistic. An uncertainty of a factor of a few seems far more probable. Emerson (1988) presents a good discussion of the behavior of β in the FIR and mm wavelength range and shows that crystalline grain materials are expected to have $\beta = 2$. The same FIR emissivity index is also expected for amorphous grains unless they are layered, in which case $\beta = 1$. Emerson (1988) also argued that based on causality any grain material had to obey $\beta \geq 1$ in the long wavelength end of the spectrum. Early sub–mm studies, however, clearly indicated that observed β–values cloud be < 1 (Weintraub et al. 1989, Beckwith & Sargent 1991), at least in accretion disks around T Tauri stars, and were typically found to be in the range of 1–1.5 for a variety of sub–mm sources (Sandell 1989). Beckwith & Sargent (1991) argue that the long wavelength emissivity index can easily be reduced by particle shape (needles, fractal grains) or due to grain composition. These rather low (sub)mm β–indices have been confirmed in a number of observations (see e.g. Chandler 1998), and the canonical value of $\beta = 2$ has been an exception rather than the rule. It is only recently that we have actually confirmed that the dust emissivity is ~ 2 for normal interstellar dust in the quiescent cores of molecular and dark clouds (Goldsmith et al. 1997, Visser et al. 1998, Johnstone & Bally 1999, Huard et al. 1999). Because we separate the protostellar dust emission from that of the surrounding cloud and determine β directly from our observations, we can use the opacities defined at 250 μm. We note that by adopting a gas–to–dust ratio of 100, we get opacities close to the values recommended by Henning et al. (1995) at 1.3 mm. This is because we generally find a β–index of 1.4–1.5 (see below) for embedded protostellar sources, while it appears that β is close to 2 for the extended molecular cloud emission.

4.1. NGC 6334 I

NGC 6334 I has been extensively observed in the FIR, but with beam sizes at 100 μm of 40″ or more (Harvey & Gatley 1983, Loughran et al. 1986). The published flux densities therefore also include emisson from the surrounding cloud. Any realistic fit of the sub–mm data should therefore yield lower flux densities than those measured at 134 and 100 μm. NGC 6334 I is resolved in all our sub–mm maps. The 800 μm–map gives a size of $\sim 11'' \times 8''$ with a P.A. $\sim 43°$. At longer wavelengths it appears somewhat more extended, most likely due to the larger beamsize employed. A size of 8″–10″ agrees well with the size of the molecular high density core measured by McCutcheon et al. (2000) from maps of high excitation molecular transitions, and we constrain our dust fits to this range.

Since NGC 6334 I is associated with a UC HII region, we have subtracted out a point source contribution of free-free emission, by taking a flux density of 3.3 Jy for NGC 6334 I at 1.3 cm (Jackson et al. 1988) and extrapolated the flux density to shorter wavelengths assuming this to be optically thin free–free. Another complication for NGC 6334 I is that the broad band fluxes measured in our calibrated maps as well as with UKT14 photometry are severely affected by "pseudo–continuum" from compact molecular line emission centered on the hot core. The only direct measurement we have of spectral line contamination is from our RxB2 experiment (see Sect. 2.1), which suggests a line excess of 8 $\pm$ 4% at 850 μm. However, since we do not know the contribution of spectral line flux in the different sub–mm bands, we make the assumption that the line contamination is about the same in all bands. The unknown amount of line contamination in the different filters adds an additional uncertainty to our least squares fits. Neither do we include the 7 mm data from Carral et al. (1997), because the VLA observations are not sensitive to the more extended dust emission, which we see in our single dish data. The best fit to our map data is shown in Fig. 3 and predicts the dust to be marginally optically thick at 1.1 mm ($\tau_{1.1mm}$ = 0.07). The results are given in Table 3. Here we have corrected the total mass with 8% to account for line contamination. It is clear from Fig. 3 that the dust emission is not well described by an isothermal fit. The fit underestimates the flux density at 1.3 mm, presumably because the cooler envelope becomes optically thin and we see a larger contribution from hotter dust. It overestimates the observed flux density at 60 μm, because here the emission is dominated by the cool envelope, and the fit therefore also overestimates the bolometric luminosity. Because we cannot describe I very well with an isothermal fit, we estimate that the mass is uncertain by at least 50%. The central core in NGC 6334 I is very hot. McCutcheon et al. (2000) find molecular emission from energy states as high as 900 K and Mangum & Wootten (1993) deduce a gas temperature of 295 K from their multi–transition H_2CO analysis.

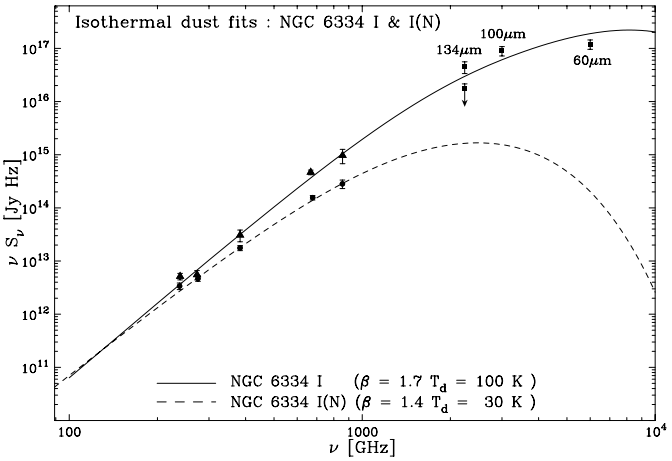

Fig. 3. Isothermal fits to the continuum emission from NGC 6334 I and I(N). The filled triangles show the flux densities of I estimated from our maps with the free–free emission subtracted. The filled circles give the flux densities for I(N). The filled squares show the 134 μm–data from Loughran et al. (1986) as well as the 100 μm and 50 μm–data from Harvey & Gatley(1983). We have marked the 134 μm–data point for I(N) as an upper limit, since the Loughran et al. (1986) data refer to the flux density in a $\sim 1'$-beam, which therefore includes a large part of the dense cloud core surrounding I(N).

4.2. NGC 6334 I(N)

The strong sub–mm source I(N) is a special case. Early (sub)mm observations were done with broad beams (Cheung et al. 1978, Gezari 1982) and included the whole I(N) molecular cloud core. The approximate diameter of the I(N) cloud core is $\sim 100''$, i.e about twice the beam size of these early observations. NGC 6334 I is not surrounded by a large dust cloud and since the compact dust core has a size $\leq 10''$, the dust emission will be severely diluted in a $65''$ beam. Therefore it is not surprising that Gezari (1982) found that I(N) was brighter than I at 1 mm and he therefore concluded that I(N) was extremely cold. When observed with similar resolution in the mm and sub–mm band, I(N) is fainter than NGC 6334 I at all frequencies (Table 2), and more so than I at shorter wavelengths. Fig. 4 shows more detailed sub–images of the I(N) cloud core. The I(N) cloud core contains at least two compact sources, I(N) and SM 2, both of which are extended. We have retained the name I(N) for the bright sub–mm source in the northern part of the cloud core. There may be a fainter source $\sim 10''$ SW of I(N), c.f. Fig. 4, especially the 800 μm and the 450 μm–images, but we do not have accurate enough data to confirm it. NGC 6334 I(N) is faint in the FIR. It is detected in the 134 μm–map of Loughran et al. (1986), where it is seen as a lobe of relatively faint emission extending to $\sim 2'$ north of I, and it is even marginally present in their 71 μm–map.

In this case we have to separately treat I(N), SM 2, and the surrounding cloud core. These three source components should not exceed the FIR luminosity estimated by Loughran et al. (1986), 6.5 10^4 $L_\odot$. For I(N) this is not a very stringent constraint. The emission from the surrounding cloud core can easily explain the observed luminosity if the gas and dust are thermalized, i.e. if we assume a dust temperature of 30 K. This is the gas temperature that Kuiper et al. (1995) deduced from their NH_3 observations. We know from molecular line observations that I(N) is cold, since it was not detected in any of the high excitation lines, which are seen in abundance towards NGC 6334 I (McCutcheon et al. 2000). There is some evidence for hot gas in the center of I(N), both from the presence of the CH_3OH maser and from the detection of NH_3(6,6) emission (Kuiper et al. 1995), but the emission from the hot dust will be absorbed by the cooler envelope. The average dust temperature is therefore likely to be ≤ 40 K, but not colder than 30 K, since Kuiper et al. (1995) find a gas temperature of 30 K and McCutcheon et al. (2000) derive 32 K from their LVG analysis. We find that we can get plausible fits to the dust emission in the range of 30–35 K. All the parameter space we explored ($25\,\mathrm{K} \leq T_d \leq 40\,\mathrm{K}$) shows that the dust emission is already somewhat optically thick at 1.1 mm ($\tau_{1.1\mathrm{mm}} \geq 0.1$). The best least squares fit, constrained to T_d = 30 K, gives $\tau_{1.1mm}$ = 0.23, and the results of the fit are summarized in Table 3. We can see from Fig. 3 that although the fit appears quite good, it underestimates the 1.3 mm flux, almost certainly because we see more hot gas at long wavelengths.

We do not have enough data to make a proper least squares fit to SM 2, because the source is relatively faint and located in a region of intense cloud emission. We therefore assume the same dust temperature and β–index that we found for I(N) and use the measured flux densities 450 and 350 μm to derive a mass (Table 3).

Table 3. Mass estimates obtained from isothermal fits to the total flux densities in Table 2 and contrained to the source sizes given in Table 1. The uncertainty in mass is $\sim$ 50%, and in $\beta \sim 0.3$. These errors are largely due to the uncertainty in dust temperature, T_d, which is not well constrained, see text.

SOURCE	M_{tot} ($M_\odot$)	T_d (K)	β	n (cm^{-3})	L_{bol} ($L_\odot$)
I	200	100	1.7	1.2 10^7	2.6 10^5
SM1	175	25	2.0	5.2 10^6	1.2 10^3
SM2	70	30	1.5	3.5 10^6	1.2 10^3
SM3	100	22	1.5	4.6 10^6	0.4 10^3
I(N)	400	30	1.4	2.6 10^7	1.9 10^3
SM4	120	24	2.0	6.0 10^6	0.4 10^3
SM5	120	25	2.0	2.4 10^6	0.4 10^3
SM6	100	20	1.4	2.8 10^6	0.2 10^3
SM7	130	25	2.0	9.1 10^5	0.4 10^3
SM8	80	25	2.0	1.8 10^6	0.2 10^3

We can also estimate a total mass for the cloud core surrounding I(N), i.e. the region bounded in the north about halfway between I(N) and SM 4, in the south between SM 2 and SM 1, in the west across the ridge connecting it to the linear filament, or an area of $\sim 2.5' \times 1.5'$. The mm–maps are expected to measure the total flux more correctly than the ones at 350 and 450 μm (Sect. 2.1). If we do a straight fit to the 1.3 mm – 800 μm flux densities (Table 2), we get a dust emissivity β = 1.75 and a temperature of $\sim$ 30 K. If we force the dust emissivity to β = 2, then the fit gives a dust temperature, $T_d \sim 19$ K. The first fit would essentially explain the luminosity observed toward the I(N) region (L_{bol} = 5.2 10^4 $L_\odot$), while the latter underestimates the measured FIR luminosity. If we ignore the sub–mm data and use β = 2, we find $T_d \sim 27$ K, and a total mass of 2200 $M_\odot$ for the surrounding cloud or a visual extinction of several hundred magnitudes through the cloud core. If we include the mass of the two embedded sources, we find that the whole I(N) region has a mass of $\sim$ 2700 $M_\odot$. This mass estimate agrees surprisingly well with what Kuiper et al. (1995) derived from their NH_3 observations, $\sim$ 3000 $M_\odot$.

4.3. Other sources and total cloud mass

The rest of the compact sources listed in Tables 1 & 2 are fainter than the ones discussed above. Their flux densities are much more uncertain, because they are located in ridges, where it is difficult to separate the background emission from that of the source. Neither do we know much about these sources, because none of them are seen in the FIR, and high resolution molecular line observations of the region are extremely scarce. SM 1, which lies on the ridge connecting I to the I(N) cloud core, is quite bright at 450 and 350 μm, but looks inconspicuous in the CS J = $7-6$ map by McCutcheon et al. (2000). There is some high velocity gas close to it, but probably unrelated to SM 1.

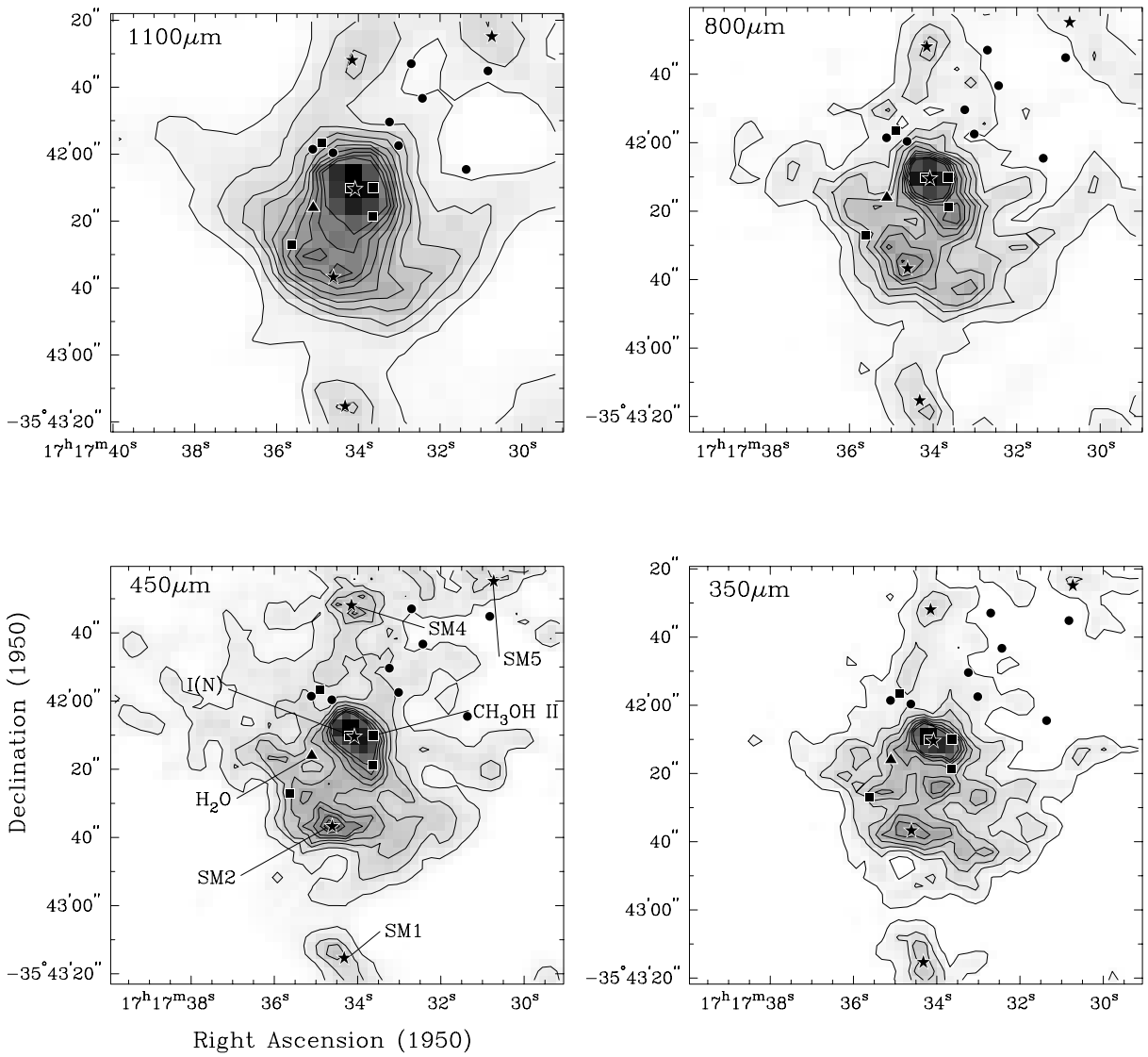

Fig. 4. Closeup view at high resolution of the I(N) core at 1100 μm, 800 μm, 450 μm, and 350 μm. The 1100 μm and 800 μm images are restored to a 5″ beam, and have peak flux densities of 2.67 and 10.7 Jy/beam, respectively. The ten contours are linear, starting at 5% of the peak flux density with a step of 5% of the peak. The 450 μm and 350 μm images are restored to a 3″ beam, and have peak flux densities of 22.7 and 48.1 Jy/beam, respectively. The eight contours are linear starting at 6% of the peak flux density with a step of 6% of the peak. All four images are enhanced with a grey scale going to 90% of the peak flux density. The positions of the sub–mm sources in the field are marked by filled star symbols and labelled on the 450 μm image. The position of the Class II CH_3OH maser (Norris et al. 1998) is marked by a filled square and labelled CH_3OH II on the 450 μm image. The positions of the main Class I CH_3OH maser clusters (Kogan & Slysh 1998) are also marked with filled squares, while the position of the H_2O maser (Moran & Rodríguez 1980) is marked by a filled triangle. The positions of the vibrationally excited H_2 emission knots (Megeath & Tieftrunk 1999) are marked with filled circles.

The same is true for SM 4, north of I(N), suggesting that they both are relatively cold. Dust fits to both sources suggest $\beta \sim 2$. We therefore constrained β =2, which give T_d in the range 22–25 K. SM 6 appears to have a flatter emissivity law and be even colder, but the 450 μm-data are rather uncertain and the β-index could well be higher. For SM 5, SM 7 and SM 8 we have no 450 μm-data, and for these we assume T_d = 25 K, and a β = 2, i.e. similar to what we found for SM 1 and SM 4.

McCutcheon et al. (2000) draw attention to the ridge northwest of NGC 6334 I, which they call I(NW). This ridge is very bright in CO J=3 – 2 and CS J=7 – 6 and appears to be associated with high velocity gas, but it is not part of the outflow that was originally discovered by Bachiller & Cernicharo (1990). The ridge connects I to the HII region E, which has little, if any dust emission. There is no indication in our data that this ridge would contain any compact sources. However, because the ridge is so close to I, the morphology deduced from the DBMEM reduction is rather uncertain. At 800 μm, see Fig. 2, the ridge appears double peaked, while at other wavelengths it looks like a single source. The double–peaked structure at 800 μm is therefore al-

most certainly an artifact of the data reduction. In this case we assume a dust temperature of 50 K, because the ridge is connecting to the high luminosity source I and very bright in CS J = 7 − 6, suggesting that it is hot. If we further assume β = 2, we find a mass of $\sim 250\,M_\odot$ for I(NW) based on our 1.3 and 1.1 mm observations.

Since we have maps at several wavelengths, we can derive a total mass of the whole northern part of NGC 6334 covered by our maps. We know that the dust temperature is by no means constant over the cloud, because near I and E we have HII regions heating the dust, whereas there are no known luminous sources in the northern part of the cloud. To some extent we can account for temperature variations by subtracting out the most prominent sources in our map, and assume a constant dust temperature for the rest. CO observations (McCutcheon et al. 2000) suggest that 30 K may be a reasonable assumption. Both the 1.3 mm and 1.1 mm maps give very similar results, i.e. a cloud mass of 1.13 $10^4\,M_\odot$, or a total mass of 1.2 $10^4\,M_\odot$, when we add the sources treated separately.

5. Discussion

5.1. The formation of a high mass cluster

Our observations show that the dust emission in the northern part of NGC 6334 is very filamentary and lumpy. The morphology of the dust emission looks remarkably similar to numerical models of isothermal gravitational collapse and fragmentation of a molecular cloud (Klessen et al. 1998). Their model calculations show that once a molecular cloud becomes gravitationally unstable, it tends to collapse into filaments and knots. The most massive cores form at the connecting nodes of the filaments, which in NGC 6334 would be represented by regions like I and I(N). Filamentary structures are quite common in cluster forming molecular clouds. In this respect NGC 6334 is no exception. Orion A, the nearest and best studied high mass star formation region, shows numerous arcs and filaments extending over more than 50′ on the sky (Chini et al. 1997, Johnstone & Bally 1999). Similar filamentary structure is seen in DR 21 (OH), another high mass star formation complex (Wilson & Mauersberger 1990, Mangum et al. 1992, Chandler et al. 1993). Even molecular clouds that form only low to intermediate mass stars, like ρ Ophiuchus (Motte et al. 1998, Wilson et al. 1999) show the same kind of filamentary knotty structure, suggesting that the collapse and fragmentation of a molecular cloud is not a strong function of the mass of the cloud.

As in other high mass star forming regions, NGC 6334 I also appears to form low and intermediate mass stars. The near–IR survey by Straw et al. (1989) and Straw & Hyland (1989) revealed a high proportion of objects with infrared excess near NGC 6334 I, which they interpreted as a very young, compact cluster with a diameter of $\sim$ 1 pc. Tapia et al. (1996) repeated their work using a near–IR camera, and cloud therefore go considerably deeper than the survey done by Straw et al. (1989), which was done by scanning with a single pixel detector. Tapia et al. (1996) confirm the presence of an embedded, young stellar cluster centered on NGC 6334 I with a size of $\sim 70''$ (0.6 pc), a stellar density of $1200\,\mathrm{pc}^{-3}$ and estimated the star formation efficiency to be $\sim$ 25%. This estimate appears to be too high, since we find that the total mass (gas & dust) is about 3 times higher than what they used. The present star formation rate is apparently low in the northern part of NGC 6334, but the presence of the sub–mm protostellar sources suggests that the future rate will be much higher. Tapia et al. (1996) find that the apparent stellar density falls off to the north and and northwest, presumably mostly due to the high extinction areas we see in our sub–mm maps (Fig. 1 & Fig. 2). They hardly find any near–IR sources toward the I(N), partly because of the extremely high extinction in the I(N) cloud core, but also because I(N) is younger and just in the process of forming stars. The mass of the I(N) cloud core and the presence of several massive protostellar sources in the core suggests that this cloud is likely to give birth to another stellar cluster.

5.2. The strong sub–mm sources NGC 6334 I, I(N) and SM 2

The sub–mm sources trace a younger population of stars than the ones we see in the near– or mid–infrared. Some of the sources in Table 1 may not even be gravitationally bound, but the strongest ones are either associated with young massive stars or represent massive protostellar sources. We call a sub–mm source protostellar, if it is clear that the source is gravitationally unstable and has a formed a stellar core, either seen due to free–free emission, outflow activity, or manifested by maser emission in H_2O or CH_3OH. A protostellar source may contain one or several protostars, while a protostar is an object which derives more than half of its energy from accretion (Beichman et al. 1986). We call a sub–mm source prestellar if we have found no evidence that it has formed a stellar core, and if it is unclear whether the source is gravitationally unstable, gravitationally bound or unbound. A prestellar core is essentially identical to a starless core (Benson & Myers 1989) or what Ward-Thompson et al. (1994) call a pre-protostellar core. It may already be in a state of collapse, but it is also possible that a prestellar core is unbound, i.e. it could just be a transient density condensation.

The sub–mm source NGC 6334 I coincides with the FIR position and the two 20 μm sources IRS−1 and IRS−2 (Harvey & Gatley 1983) as well as with the cometary type UC HII region NGC 6334 F (also called G351.42+0.64) (Rodríguez et al. 1982, Gaume & Mutel 1987, De Pree et al. 1995), and the hot NH_3 core (Kraemer & Jackson 1995). This is illustrated in Fig. 5, which shows that with the resolution that we can achieve in our single dish observations, we can not resolve the individual protostars from the UC HII region or the hot core. The cometary HII region F is believed to be powered by IRS–1 (Harvey & Gatley 1983), which is close, but not necessary coincident with one of the CH_3OH masers (Ellingsen et al. 1996, Norris et al. 1998). The second CH_3OH maser is close to IRS−2, the protostellar object found by Harvey & Gatley 1983). McCutcheon et al. (2000) find two molecular outflows, possibly powered by the two protostars seen as Class II methanol masers. NGC 6334 I therefore harbours at least two young stars. The virial mass for I is $\sim 40\,M_\odot$, estimated from data in McCutcheon et al. (2000),

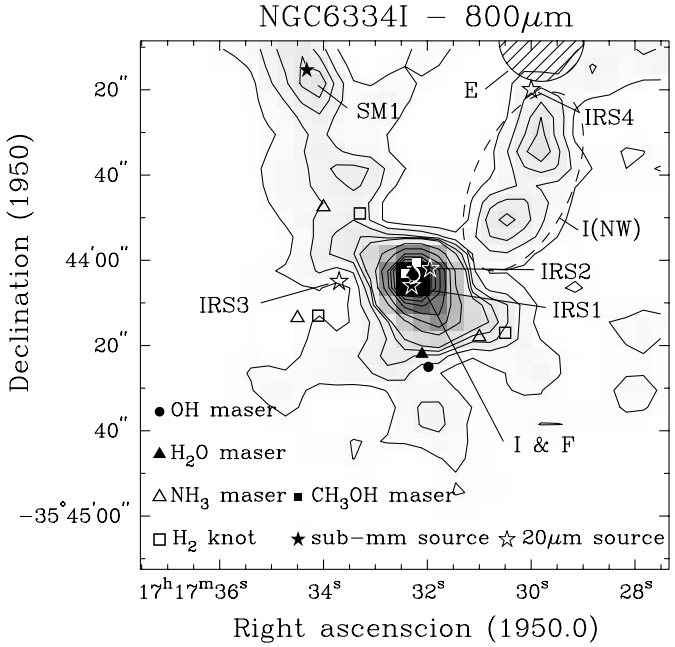

Fig. 5. Closeup view of NGC 6334 I at 800 μm plotted with greyscale and overlayed with contours. The 800 μm image is restored with a 6″ beam and has a peak flux of 26.1 Jy/beam. The contour levels are 0.5, 1, 1.5, 2, 2.5, 5, 7.5, 10, 12.5, 15, 17.5, 20, and 25 Jy/beam. In the north we see the ridge source SM 1 and in the northwest half of the evolved HII region E (Rodríguez et al. 1982). E connects to I through the dust ridge labelled I(NW) by McCutcheon et al. (2000), which here looks like a double source. In other maps it looks much smoother and hence the appearance of a double source is an artifact of the data reduction. All the activity in I takes place within the region of intense sub–mm emission.

while the sub–mm continuum predicts a mass of $\sim 200\,M_\odot$ (Table 3), suggesting that the sub–mm core is gravitationally unstable and in a state of collapse. It may already have given birth to one protostellar source, IRS$-$2, or possibly two sources, if the CH_3OH maser is unrelated to IRS$-$2. NGC 6334 I is therefore a hot core, which already harbours at least one protostellar object, and which is likely to form additional stars. In this respect NGC 6334 I resembles the hot core region W3(H_2O), which contains at least two protostellar sources and possibly additional low–mass pre–main–sequence stars (Wilner et al. 1999).

NGC 6334 I(N) is another, even more extreme protostellar source. Our sub–mm maps show that the protostar has a size of $\leq 10''$ corresponding to a radius of ~ 0.04 pc. At shorter wavelengths it becomes more elliptical (see Fig. 4). I(N) is not detected in the free–free (Rodríguez et al. 1982), i.e. it has no associated HII region, yet our sub–mm observations suggest that it has a mass of 250–400 $M_\odot$. The mass derived from dust observations is far larger than the virial mass, which is $\sim 30\,M_\odot$, estimated from the linewidth of $H^{13}CO$ J=4 – 3, which is $3.7\,\mathrm{km\,s^{-1}}$ (McCutcheon et al. 2000). I(N) drives a bipolar outflow, seen both in CO J=3 – 2 and CS J=7 – 6 (McCutcheon et al. 2000) and in several SiO transitions (Megeath & Tieftrunk 1999). Megeath & Tieftrunk (1999) find eight knots of shock–excited H_2 emission north of I(N). One of their H_2 emission knots coincides with the red K–band nebulosity #229 (Tapia et al. 1996), suggesting that the broad band K emission is due to vibrationally excited H_2 emission. All H_2 knots are outside the dense molecular cloud core (Fig. 4), where the extinction is expected to be moderate. I(N) is associated with an H_2O maser (Moran & Rodríguez 1980) and several Class I CH_3OH maser spots (Kogan & Slysh 1998). It coincides with a Class II CH_3OH maser (Norris et al. 1993, Ellingsen et al. 1996, Norris et al. 1998). Since Class II methanol masers are believed to trace the accretion disks around massive stars (Norris et al. (1998), the presence of a Class II maser would therefore indicate that I(N) has already formed a hot accretion disk. Yet NGC 6334 I(N) is completely invisible even at 60 μm, which suggests that it is very cold and extremely obscured. It is marginally seen in the 134 μm–map of Loughran et al. (1986), where it shows up as lobe of relatively faint emission extending to $\sim 2'$ north of I. However, it cloud well be that the 134 μm emission traces more of the massive surrounding cloud core than emission from I(N) itself. Our mass estimate (see Sect. 4.2) and the observed size of I(N) predict a line of sight (l.o.s.) visual extinction of 2000^m - 3000^m, which explains why I(N) has remained undetected in the mid–IR.

NGC 6334 I(N) has in fact all the characteristics of a high–mass Class 0 object as defined for low mass objects by André et al. (1993). It has no detectable HII region, no near or mid–IR counterpart, it is associated with a Class II methanol maser and drives a bipolar outflow. The protostellar envelope is extremely massive, M = 250–400 $M_\odot$, but the bolometric luminosity is relatively modest, $L_{\rm bol} \leq 3\ 10^3\,L_\odot$. A large fraction of this luminosity is radiated in the sub–mm. The ratio of sub–mm (i.e. radiation shortward of 900 GHz) to bolometric luminosity $L_{\rm submm}/L_{\rm bol} \geq 3\ 10^{-2}$. The outflow is not highly collimated, which is typically a characteristic of Class 0 objects, but even for low mass Class 0 objects there is quite a spread in outflow properties (Bachiller 1996). I(N) therefore appears in any respect to be as good a candidate for a high mass class 0 object as IRAS 23385+6053, which was recently suggested by Molinari et al. (1998) to be a prototype high–mass class 0 object. Both objects have similar envelope masses, no radio or mid–IR emission, and radiate a large fraction of their luminosity in the sub–mm regime. However, these two high mass protostars are not by any means unique. Using similar arguments one cloud also indentify several of the continuum sources in DR 21(OH) as massive protostars (Mangum et al. 1992, Chandler et al. 1993). Another good candidate is IRAS 20126+4104 (Cesaroni et al. 1997), where Zhang et al. (1998) find evidence for a massive, rotating Keplerian disk. However, the mass of this "isolated" protostar is only $\sim 20\,M_\odot$, which is roughly about the same mass that Cernicharo et al. (1998) found for "isolated" protostars in the Trifid Nebula. Isolated high mass protostellar sources therefore appear less massive than those found in molecular clouds forming clusters, like NGC 6334 or DR 21(OH).

However, we do not expect I(N) to form a 200 $M_\odot$ star. If the accretion core reaches a mass of $\sim 10\,M_\odot$, radiation pressure from the protostar will halt the accretion and thus limits the mass, see e.g. Bonnell et al. (1998). It is therefore much more

likely that I(N) will form several stars, rather than a single massive star. If massive stars form through collisions (Bonnell et al. 1998, Stahler et al. 1999) then I(N) cloud be a good candidate for forming a massive star. For this to happen, it seems that the ideal conditions would be a very dense protostellar core, which simultaneously collapses and fragments into several protostars. If one massive star forms much earlier than the rest, then it is likely to halt the collapse of nearby companions and thus limit the formation of more massive stars. This cloud be what happened in I, where IRS$-$1 formed first, and where we are not likely to find any stars more massive than IRS$-$1.

I(N) has not formed a massive ionizing star. The protostellar core is cold, yet it has extreme gas densities. There is some evidence that it may already have formed more than one star, but this evidence is not very secure. We would expect the accretion core to be centered on the sub-mm source, yet the Class II CH_3OH maser is offset from the peak emission (Fig. 4). The Class I CH_3OH maser spots (Kogan & Slysh 1998) are difficult to reconcile with the observed molecular outflow, unless the outflow is very poorly collimated. The positions and the velocities of the individual maser spots would make more sense if there was more than one outflow. Neither do the H_2 emission knots align up very well with the outflow. Megeath & Tieftrunk (1999) therefore interpret the alignment of some of the H_2 emission knots as being powered by a separate source than the protostar driving the CO and SiO outflow. If their interpretation is correct, the exciting star for the H_2 knots would not coincide with I(N), but be more to the north, where the dust emission is relatively faint. Therefore, even though we cannot say whether the sub–mm source I(N) hosts multiple protostars, it seems clear that the massive I(N) cloud core contains more than one protostellar object. As mentioned earlier (Sect. 4.2) we find some evidence for a fainter source southwest of I(N). South of I(N) there is also the massive sub–mm source SM 2, which is very likely a protostellar source. However, since no maser or free-free emission has been seen toward SM 2, we have no information that cloud tell us whether this source already has a stellar core. The CS J=7-6 map by McCutcheon et al. (2000) does show some high velocity emission in the direction of SM 2. Whether this high velocity gas originates from SM 2, or whether it is part of the I(N) outflow will have to be confirmed by more detailed mapping at high spatial resolution.

We therefore support the suggestion by Megeath & Tieftrunk (1999), who propose that the I(N) cloud core is in a very early stage of cluster formation. The I(N) cloud core is indeed likely to form a cluster of mostly low and intermediate mass stars. Megeath & Tieftrunk argue that in I(N) at least one intermediate to high mass star have formed before the appearance of a dense low mass cluster, but whether this is implies that high mass stars generally form first is still unclear.

5.3. The new sub–mm sources

The nature of the other sub–mm sources we identify in our maps is much less certain. The most detailed molecular line observations made to date with high spatial resolution are those of McCutcheon et al. (2000), who mapped most of the I and I(N) cloud core in CS J=7 $-$ 6 and made partial maps in $C^{17}O$ J=3 $-$ 2, but the maps only cover SM 1, SM 2 and SM 4. In our 350 μm–image SM 1 appears very elongated, and cloud in fact be a double source. It appears centrally condensed, which would suggest that it is a protostar. Protostellar sources have much steeper density gradients than prestellar cores, which appear to have rather flat density distributions (Ward-Thompson et al. 1994). The CS J=7-6 map by McCutcheon at al. (2000) does not show an enhancement of CS at the position of SM 1, suggesting that the source is cold. The linewidth of the CS emission is ~ 3.6 kms^{-1}, which corresponds to a virial mass of 25–40 $M_\odot$, and hence it appears gravitationally unstable. SM 1 is therefore either a protostar or a prestellar core that will collapse into a protostar. The measured spectral energy distribution is rather steep with a $\beta \sim 2$, which would make it a prestellar core rather than a self–luminous source. SM 4, the compact source $\sim 20''$ north of I(N) is not detected in CS J=7 $-$ 6 by McCutcheon et al. (2000), suggesting that this is another cold source. This source is also likely to be gravitationally unstable and therefore a potential protostar, even though the derived β–index would suggest that it is more likely to be a prestellar core. Both SM 1 and SM 4, however, are located on narrow dust ridges. This makes it very difficult to determine accurate flux densities, especially at longer wavelengths where the beam is large and the source emission faint and of the same order as the underlying dust ridge. Our observations are not accurate enough to say whether SM 1 and SM 4 are protostars or prestellar cores. We need to to re–observe them with better S/N, but we also need molecular line observations that can give us the temperature and velocity information of the gas surrounding these sources.

There is even less we can say about the sub–mm sources further north. The dust emission is fainter and our maps (with the exception of the 800 μm–map) have higher noise levels, which make the flux densities much more uncertain. Neither do we have any 450 or 350 μm observations, or any supporting molecular line observations. The low resolution CO map by Dickel et al. (1977) shows that the northernmost part of NGC 6334 is colder, which is probably true in the light of the much fainter sub-mm emission seen in this area. Several of the sources listed in Tables 1 & 2 are part of the linear filament. These are also massive cores, probably in a very similar evolutionary state to SM 1, and SM 4, i.e. they are likely to either be cold, relatively massive protostellar sources or massive prestellar cores.

5.4. The linear filament

The linear filament is another enigmatic feature in our maps. Filamentary structure in interstellar space is relatively common, see e.g. Schneider & Elmegreen (1979) who give a catalog of 23 dark cloud filaments. Sub–mm maps of the ρ Ophiuchi dark cloud (Wilson et al. 1999) and Orion (Johnstone & Bally 1999) also show linear features, but the ρ Ophiuchi filaments are rather faint and smooth, while the Orion A integral filament is quite extended and breaks up into a number of star forming condensations. In that respect the Orion integral filament appears more

similar to the linear filament seen in NGC 6334 and the dark cloud filaments catalogued by Schneider & Elmegreen (1979). The latter often look windswept and wiggly, and they break up into condensation that are likely to collapse into stars.

However, what is so remarkable with the NGC 6334 linear filament is that it appears perfectly straight over the whole map, c.f. the 800 μm–map in Fig. 2. There is no sign of bending or curvature. The filament does break up into condensations with a separation between the condensations of about 2–4 times the width of the filament. Two of these condensations (SM 3 & SM 6) are listed by us as compact sub–mm sources. This separation to width ratio is very similar to that found by Schneider & Elmegreen (1979), 3 ± 1, which suggests that the fragmentation of the NGC 6334 linear filament follows the same fragmentation process as the dark cloud filaments. However, this does not explain how the filaments were formed in the first place. Aligning such a large structure as the linear filament strongly suggests that it must at some point have been magnetically supported. Nakajima & Hanawa (1996) note that in some clouds the magnetic field appears perdendicular to the axis of a filamentary cloud, while in others the magnetic field is parallel to the filament. they show that a filamentary cloud is easily formed by collapse and fragmentation of a magnetized sheet–like cloud. In their model the cloud collapses along the field lines, while the magnetic field gets amplified and runs almost parallel with the filament inside the filament. This inner parallel magnetic field supports the the filament against collapse for a time period much longer than the free–fall time, although even a magnetized filament is expected to fragment in the direction of the axis by gravitational instability. Whether this process can create a filament which is as long and straight as the filament we see in NGC 6334 is not clear.

6. Conclusions

The continuum maps reveal intense dust emission over most of the area mapped, which is very filamentary and lumpy. The strongest dust emission at all wavelengths originates from a compact source near or coincident with the UCHII - region NGC 6334 F and the FIR–source NGC 6334 I. There is a ridge of dust emission connecting NGC 6334 I to NGC 6334 I(N), the cold protostellar core discovered by Gezari (1982). We resolve Gezari's cold source into a compact (deconvolved FWHM $\sim$ 10″) dust source, which appears optically thick even at 1.1 mm. I(N) is embedded in a dense cloud core, $\sim 2.5' \times 1.5'$. There is at least another protostellar candidate, SM 2, in the large I(N) cloud core. SM 2 is $\sim 30''$ to the south of I(N).

I(N) is clearly a high–mass Class 0 object, but about two orders of magnitudes more massive than ordinary Class 0 objects, which are believed to be low mass protostars. It emits a large fraction of its luminosity in the sub–mm ($L_{bol} \sim 1.7\ 10^4\ L_\odot$), drives a molecular outflow and is associated, but not coincident with an H_2O maser. The sub–mm core coincides with a CH_3OH maser, suggesting that I(N) has already formed a hot accretion disk. We derive a total mass (gas + dust) of 250–400 $M_\odot$, corresponding to an average gas density 1.6–2.6 10^7 cm^{-3} and a l.o.s. visual extinction of $\geq 2000^m$, rendering it impossible to detect I(N) even in the thermal or mid–IR. The nature of the southern sub–mm source SM 2 is more uncertain, but it may be another massive protostar with a mass of $\sim 70\ M_\odot$. The sub–mm cloud core, including the two protostellar regions has a mass $\sim$ 2700 $M_\odot$.

The dust envelope surrounding NGC 6334 I is much hotter, $T_d \geq 100$ K, and has a total mass (gas + dust) of $\sim 200\ M_\odot$. It is more evolved than I(N) and much more active. It drives two powerful bipolar outflows, excites maser emission in OH, H_2O, CH_3OH and NH_3, and harbours at least two protostellar objects or young stars. It is associated with a hot molecular core, which is an extremely rich source of molecular line emission. A nearby HII region E, is connected to I by a bridge of strong dust emission. This HII region is powered by a cluster of B–type stars, and is associated with very little dust emission, suggesting that it is more evolved than I and I(N).

In addition to the strong sub–mm source I and the two sources I(N) and SM 2 in the large I(N) cloud core, we identify another seven compact sub–mm sources. Whether these sources are high–to–intermediate mass protostars is not clear from the present study. They may be massive cold starless cloud cores that eventually may collapse to form stars.

Our sub–mm maps also show a remarkable narrow, lumpy, linear filament, which has no optical or near–IR counterpart. This filament bounds the dust emission to the west and is at least 7′ (3.5 pc) in length with a width of $\sim 15''$–$20''$. It breaks up into dense condensations with a separation of 3–4 times the width of the filament. The filament is approximately parallel with the galactic plane. The nature of this filament is unclear, but there is no evidence that it would have been caused by the ongoing star formation activity in NGC 6334. It is more likely a pre–existing structure, where the dust condensations now may be in a stage of gravitational collapse.

Acknowledgements. I would like to thank Dr. Fred Baas, who was a collaborator with me in the early stages of this project and made sure that we got the observing time. I also want to thank Dr. Tom Megeath for valuable discussions and for providing me with unpublished data and Malcolm Walmsley for a critical reading of the manuscript. Finally, I want to thank the anonymous referee, whose insight and valuable suggestions considerably improved the paper.

References

André P., Ward-Thompson D., Barsony, M., 1993, ApJ 406, 122
Bachiller R., Cernicharo J., 1990, A&A 239, 276
Bachiller R., 1996, ARA&A 34, 111
Beckwith S.V.W., Sargent A.E., 1991, ApJ 381, 250
Beichman C.A., Myers P.C., Emerson J.P., 1986, ApJ 307, 337
Benson P.J., Myers P.C., 1989, ApJS 71, 89
Bonnell I.A., Bate M.R., Zinnecker H., 1998, MNRAS 298, 93
Carral P., Kurtz S.E., Rodríguez L.F., De Pree C., Hofner P., 1997, ApJ 486, L103
Cernicharo J., Lefloch B., Cox P., et al., 1998, Sci 282, 462
Cesaroni R., Felli M., Testi L., Walmsley C.M., Olmi L., 1997, A&A 325, 725
Chandler C.J., Gear W.K., Chini R., 1993, MNRAS 260, 337
Chandler C.J., 1997, In: Woodward C.E., Shull J.M., Thronson H.A. (eds.) ORIGINS. ASP Conference Series Vol. 148, ASP, p. 237

Cheung L., Frogel J.A., Gezari D.Y., Hauser M.G., 1978, ApJ 226, L149
Chini R., Reipurth B., Ward-Thompson D., Bally J., Nyman L.-Å., Sievers A., Billawala Y., 1997, ApJ 474, L135
Davis C.J., Eislöffel J., 1995, A&A 300, 851
De Pree C.G., Rodríguez L.F., Dickel H.R., Goss W.M., 1995, ApJ 447, 220
Dickel H.R., Dickel J.R., Wilson W.J., 1977, ApJ 217, 56
Draine B.T., 1990, In: Thronson Jr. H.A., Shull J.M. (eds.) The Interstellar Medium in Galaxies. Kluwer, Netherlands, p. 483
Duncan W.D., Robson E.I., Ade P.A.R., Griffin M.J., Sandell G., 1990, MNRAS 243, 126
Ellingsen S.P., Norris R.P., McCulloch P.M., 1996, MNRAS 279, 101
Emerson D.T., Klein U., Haslam C.G.T., 1979, A&A 76, 92
Emerson J.P., 1988, In: Dupree A.K., Lago M.T.V.T. (eds.) Proc. NATO Advanced Study Institute, Formation and Evolution of Low Mass Stars. Reidel,Dordrecht, p. 193
Forster J.R., Caswell J.L., 1989, A&A 213, 339
Gaume R.A., Mutel R.L., 1987, ApJS 65, 193
Gezari D.Y., 1982, ApJ 259, L29
Goldreich, P., Kwan J., 1974, ApJ 189, 441
Goldsmith P.F., Bergin E.A., Lis D.C., 1997, ApJ 491, 615
Haslam C.G.T., 1974, A&AS 15, 333
Harvey P.M., Gatley I., 1983, ApJ 269, 613
Henning Th., Michel. B., Stognienko R., 1995, Plan. Space Science 43, 1333
Hildebrand R.H., 1983, QJRAS 24,267
Huard T., Weintraub D.A., Sandell G., 1999, ApJ 526, 833
Jackson J.M., Ho P.T.P., Haschick A.D., 1988, ApJ 333, L37
Johnstone D., Bally J., 1999, ApJ 510, L49
Klessen R.S., Burkert A., Bate M.R., 1998, ApJ 501, L205
Kogan L., Slysh V., 1998, ApJ 497, 800
Kraemer K.E., Jackson J.M., 1995, ApJ 439, L9
Kuiper T.B.H., Peters III W.L., Foster J.R., Gardner F.F., Whiteoak J.B., 1995, ApJ 446, 692
Loughran L., McBreen B., Fazio G.G., et al., 1986, ApJ 303, 629
Mangum J.G., Wootten A., Mundy L.G., 1992, ApJ 388, 467
Mangum J.G., Wootten A., 1993, ApJS 89, 123
McBreen B., Fazio G.G., Stier M., Wright E.L., 1979, ApJ 232, L183
McCutcheon W.H., Kuiper T.B.H., Sandell G., et al., 2000, MNRAS accepted
Megeath S.T., Tieftrunk A.R., 1999, ApJ 526, L113
Menten K.M., Batrla W., 1989, ApJ 341, 839
Molinari S., Testi L., Brand J., Cesaroni R., Palla F., 1998, ApJ 505, L39
Moran J.M., Rodríguez L.F., 1980, ApJ 236, L159
Motte F., André P., Neri R., 1998, A&A 336, 150
Nakajima Y., Hanawa T., 1996, ApJ 467, 321
Neckel T., 1978, A&A 69, 51
Norris R.P., Whiteoak J.B., Caswell J.L., Wieringa M.H., Gough R.G., 1993, ApJ 412, 222
Norris R.P., Byleveld S.E., Diamond P.J., et al., 1998, A&A 508, 275
Nummelin A., Dickens J.E., Bergman P., et al., 1998, A&A 337, 275
Persi P., Roth M., Marenzi A.R., et al., 1996, A&A 307, 591
Richer J.S., 1992, MNRAS 254, 165
Rodríguez L.F., Cantó J., Moran J.M., 1982, ApJ 255, 103
Sandell G., 1989, In: Tenorio–Tagle G., Moles M., Melnick J. (eds.) Structure and Dynamics of the Interstellar Medium. Springer, Berlin, p. 244
Sandell G., 1994, MNRAS 271, 75
Sault R.J., Teuben P.J., Wright M.C.H., 1995, In: Shaw R.A., Payne H.E., Hayes J.J.E. (eds.) ASP Conf. Ser. 77, Astronomical Data Analysis Software and Systems IV, ASP, San Fransisco, p. 433
Schneider S., Elmegreen B.G., 1979, ApJS 41, 87
Stahler S.W., Palla F., Ho P.T.P., 1999, In: Mannings V., Boss A.P., Russell S.S. (eds.) Protostars and Planets IV, Univ. of Arizona Press, Tucson
Straw S.M., Hyland A.R., McGregor P.J., 1989, ApJS 69, 99
Straw S.M., Hyland A.R., 1989, ApJ 340, 318
Tapia M., Persi P., Roth M., 1996, A&A 316, 102
Visser A.E., Richer J.S., Chandler C.J., Padman P., 1998, MNRAS 301, 585
Ward-Thompson D., Scott P.F., Hills R.E., André Ph., 1994, MNRAS 268, 276
Weintraub D.A., Sandell G., Duncan W.D., 1989, ApJ 340, L69
Wilner D.J., Reid M.J., Menten K.M., 1999, ApJ 513, 775
Wilson T.L., Mauersberger R., 1990, A&A 239, 305
Wilson C.D., Avery L.W., Fich M., et al., 1999, ApJ 513, L139
Woody D.P., Scott S.L., Scoville N.Z., et al., 1989, ApJ 337, L41
Wright M.C., Sandell G., Wilner D.J., Plambeck R.L., 1992, ApJ 393, 225
Zhang Q., Hunter T.R., Sridharan T.K., 1998, ApJ 505, L151